PROCEEDINGS of the
23rd International Congress on Acoustics
9 to 13 September 2019 in Aachen, Germany

Acoustic emission of aeroelastic vortex-gust interactions

Huansheng Chen[(1)], Justin W. Jaworski[(2)]

[(1)]Lehigh University, USA, huc216@lehigh.edu
[(2)]Lehigh University, USA, jaworski@lehigh.edu

Abstract

The coupled interaction between an unsteady vortical flow and dynamics of an aerodynamic structure is a canonical problem for which analytical studies have been typically restricted to either static or prescribed structural motions. The present effort extends beyond these restrictions to include a Joukowski airfoil on elastic supports and its aeroelastic influence on the incident vortex, where it is assumed that all vorticity in the flow field can be represented by a collection of line vortices. An analytical model for the vortex motion and the unsteady fluid forces on the airfoil is derived from inviscid potential flow, and the evolution of the unsteady airfoil wake is governed by the Brown and Michael equation. The aerodynamic sound generated by the aeroelastic interaction of an incident vortex, shed Brown-Michael vortices, and the moving airfoil is estimated for low-Mach-number flows using the Powell-Howe acoustic analogy.

Keywords: Vortex sound, conformal mapping, Brown and Michael equation

1 INTRODUCTION

The encounter of a vortex gust with an aerodynamic body is a canonical fluid-structure interaction with implications for the prediction of transient loads on fliers and swimmers and their generation of vortex sound. For theoretical analyses in particular, the representation of how vorticity is shed into the wake to satisfy the Kutta condition at the trailing edge plays a crucial role in gust-airfoil interactions and related unsteady airfoil problems. An early model to account for the effect of vortex shedding of a delta wing was formulated by Brown and Michael (1). Their model supposes that the vorticity shed from an edge rolls up via a connecting vortex sheet into a point vortex with time-varying circulation. We refer to such vortices as Brown-Michael vortices, whose circulation is set instantaneously to satisfy the Kutta condition. The Brown and Michael equation describes the motion of the vortex tethered to the trailing edge before it is released as a free vortex into the flow. However, the original formulation does not guarantee the removal of spurious unbalanced couple on the airfoil, which is of minor concern to the fluid dynamic problem but is important for aeroacoustic predictions based on the model. Howe (2) later constructed an emended version of the Brown and Michael equation that eliminates this unbalanced couple.

Previous analytical efforts to analyze gust-airfoil interactions are typically restricted to either static or prescribed airfoil motion, with the exception of a few recent works (3, 4, 5). The present work extends to study the dynamical problem and the aerodynamic sound problem of a gust vortex past by a Joukowski airfoil under aeroelastic motions. The dynamical problem is formulated analytically and evaluated numerically using a time-dependent conformal mapping. The Brown and Michael framework models the unsteady shedding of vorticity from the airfoil into the wake, and the linear aeroelastic plunging motion of the airfoil is calculated using unsteady airfoil theory.

The remainder of the paper is organized as follows. Section 2 outlines the model scenario and its dynamic formulation studied previously by Chen and Jaworski (6) and presents the vortex sound model. Section 3 validates the analytical/numerical framework against previous acoustic results for a stationary flat plate by Manela (4). New results are then presented for the acoustic emission of a (non-flat) Joukowsky airfoil that is free to move aeroelastically under the influence of the vortical field. Section 4 contains concluding remarks for this study.

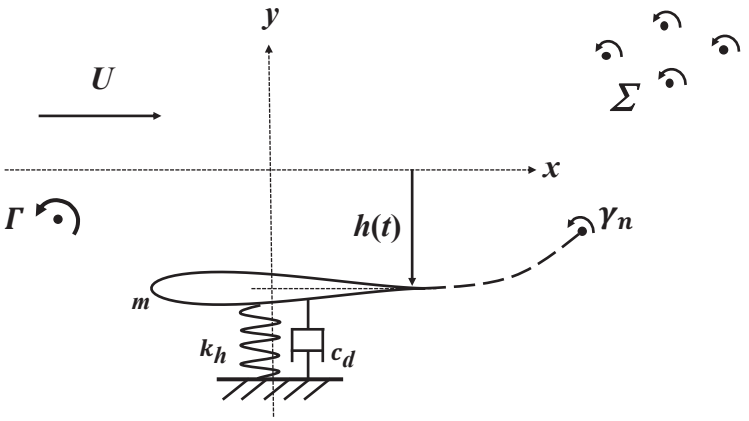

Figure 1. Schematic of the generalized model problem of an incident vortex interaction with a symmetric Joukowski airfoil on elastic translational support in a uniform flow, where U is the flow speed and $h(t)$ denotes the displacement of the airfoil. The airfoil can be considered as a damped harmonic oscillator with mass m, damping coefficient c_d, and spring stiffness k_h. Γ denotes the incident line vortex, and γ_n is the tethered trailing-edge vortex whose motion is determined by the emended Brown and Michael equation. Σ is the set of free vortices generated at the airfoil trailing edge due to unsteady airfoil loads in response to the incident line vortex or the airfoil motion. The airfoil has zero angle of attack.

2 MATHEMATICAL FORMULATION

Figure 1 illustrates the model problem of a Joukowski airfoil on elastic supports in two-dimensional uniform flow with an incident line vortex Γ and the vorticity field Σ shed into the wake. All vortices have positive circulation in the anticlockwise direction. The strength of the trailing-edge vortex γ_n satisfies the Kutta condition, and its motion obeys the emended Brown and Michael equation (2). The mathematical formulation of the aeroelastic system is now described.

2.1 Mapping

The conformal mapping of the Joukowski airfoil between the physical z-plane and the mapped ζ-plane is described by

$$\zeta(z) = \frac{1}{2}\left(z + \sqrt{z^2 - 4\lambda^2}\right) - f_0. \tag{1}$$

Using Eq. (1), the Joukowski airfoil in the physical z-plane ($z = x + iy$) with its trailing edge locating at $(2\lambda, 0)$ is mapped to a circle with radius $r = 1$ in the f-plane ($f = f_1 + if_2$), as shown in Fig. 2. Note the offset of the circle center at $f_0 = f_{x0} + if_{y0}$ and the corresponding trailing edge at $(\lambda, 0)$. For the symmetric Joukowski airfoils considered in this work, $f_{y0} = 0$. The unit circle in the f-plane is then shifted by an elementary mapping to the origin in the ζ-plane.

When time-dependent airfoil motions are considered, Eq. (1) becomes

$$\zeta(s) = \frac{1}{2}\left[s(z,t) + \sqrt{s^2 - 4\lambda^2}\right] - f_0, \tag{2}$$

where $s(z,t) = z - ih(t)$. The airfoil displacement $h(t)$ may be either prescribed or be part of the solution, as in the case of aeroelastic airfoil motions.

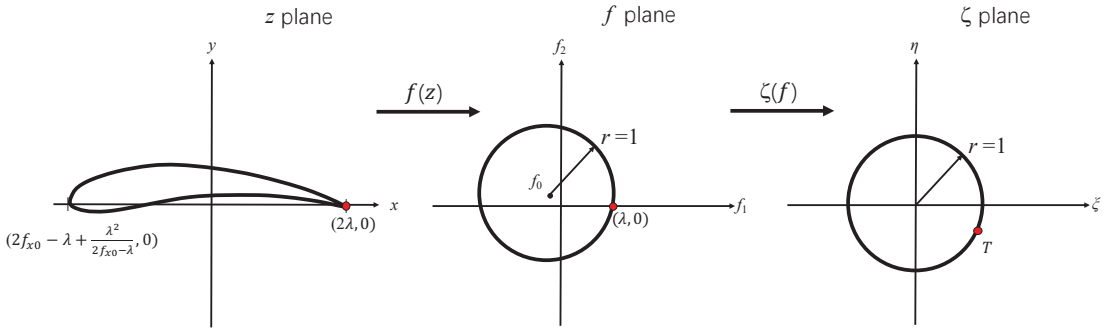

Figure 2. Successive mappings of a generalized Joukowski airfoil in the physical z-plane to a unit circle centered at the origin in the ζ-plane, T is the trailing edge location. The trailing-edge position through the successive mappings is indicated by the red dot.

2.2 Flow complex potential

The complex potential of the flow is

$$w(\zeta) = w_\gamma + w_\Gamma + w_h + U\left(\zeta + f_0 + \frac{\lambda^2}{\zeta + f_0}\right), \tag{3}$$

where $w_\gamma(\zeta)$, $w_\Gamma(\zeta)$, and $w_h(\zeta)$ are the contributions due to the shed and free vorticity field, the incident vortex, and the airfoil motion, respectively. The last term of Eq. (3) represents the uniform background flow of speed U.

The complex potential of the incident vortex $w_\Gamma(\zeta)$ is determined from the model of a vortex moving around a cylinder (7), which yields

$$w_\Gamma(\zeta) = -\frac{i\Gamma}{2\pi}\log(\zeta - \zeta_\Gamma) + \frac{i\Gamma}{2\pi}\log\left(\zeta - \frac{1}{\zeta_\Gamma^*}\right) - \frac{i\Gamma}{2\pi}\log\zeta, \tag{4}$$

where the last two terms guarantee that the total circulation inside the cylinder is initially zero, and the superscript $*$ denotes the complex conjugate. Similarly, the complex potential of the vortices shed into the wake is

$$w_\gamma(\zeta) = \sum_{k=1}^{n}\left[-\frac{i\gamma_k}{2\pi}\log(\zeta - \zeta_{\gamma_k}) + \frac{i\gamma_k}{2\pi}\log\left(\zeta - \frac{1}{\zeta_{\gamma_k}^*}\right)\right]. \tag{5}$$

By appeal to Kelvin's theorem, the bound vorticity inside the cylinder at any time has total circulation $-\sum_{k=1}^{n}\gamma_k$, which is used to compute the aerodynamic lift force.

The complex potential of the airfoil motion is (8),

$$w_h(\zeta) = iV\left(\zeta - \frac{1}{\zeta}\right), \tag{6}$$

where $V = \mathrm{d}h/\mathrm{d}t$ is the instantaneous velocity of the airfoil in the downward direction.

2.3 Vortex shedding and the emended Brown and Michael equation

The motions of the vortices shed most recently by the trailing edge are described by the emended Brown and Michael equation (2),

$$\frac{\mathrm{d}x_{\gamma_n}}{\mathrm{d}t}\cdot\nabla\Psi_j + \frac{\Psi_j}{\gamma_n}\frac{\mathrm{d}\gamma_n}{\mathrm{d}t} = v_{\gamma_n}\cdot\nabla\Psi_j, \qquad j = 1, 2, \tag{7}$$

where x_{γ_n} represents the location of a shed vortex tethered to the trailing edge with circulation γ_n, and v_{γ_n} is the fluid velocity when the local velocity induced by γ_n is excluded. Here a Cartesian coordinate system is considered, where $x \equiv (x,y)$. $\Psi_j(x,t)$ denotes the stream function of the complex potential of the flow in the j-direction. For a Joukowski airfoil mapped to the ζ-plane, the components of the stream function are (9)

$$\Psi_1 = \mathrm{Im}\{\zeta + 1/\zeta\} \quad \text{and} \quad \Psi_2 = \mathrm{Im}\{-i(\zeta - 1/\zeta)\}. \tag{8}$$

The instantaneous circulation of the tethered vortex $\gamma_n(t)$ is obtained by enforcing the Kutta condition at the trailing edge of each instant in time (6),

$$\gamma_n(t) = \frac{\left|T^*\zeta_{\gamma_n} - 1\right|^2}{\left|\zeta_{\gamma_n}\right|^2 - 1}\left(\frac{2\Gamma(1 - \mathrm{Re}\{T^*\zeta_\Gamma\})}{\left|T^*\zeta_\Gamma - 1\right|^2} - \sum_{k=1}^{n-1}\gamma_k\frac{\left|\zeta_{\gamma_k}\right|^2 - 1}{\left|T^*\zeta_{\gamma_k} - 1\right|^2} - 2\pi V\,\mathrm{Re}\{T^*\}\right), \tag{9}$$

in which T^* is complex conjugate of the trailing edge T location ($T = \lambda - f_0$) in the ζ-plane. The tethered trailing-edge vortex is released and becomes a free vortex when $\mathrm{d}\gamma_n/\mathrm{d}t$ changes sign, at which time another tethered vortex is placed at the airfoil trailing edge whose motion and instantaneous circulation are determined by Eq. (7) and Eq. (9), respectively.

Equation (7) can be rearranged into the equivalent scalar form

$$\frac{\mathrm{d}z^*_{\gamma_n}}{\mathrm{d}t} + (H_1 - iH_2)\frac{1}{\gamma_n}\frac{\mathrm{d}\gamma_n}{\mathrm{d}t} = v^*_{\gamma_n}, \tag{10}$$

where $z^*_{\gamma_n} = x - iy$ and $v^*_{\gamma_n} = v_x - iv_y$. The functions H_1 and H_2 involve the stream functions Ψ_j and their derivatives. Equation (10) is the equivalent scalar form of the emended Brown and Michael equation, which is employed for the theoretical analysis in this work. Specific details related to the derivation of Eq. (10) and the expressions of H_1 and H_2 from (6) are presented in the Appendix for reference. Also, the complex velocity of the shed vortex with self-potential velocity excluded is (7)

$$v^*_{\gamma_n} = -\frac{i\gamma_n\zeta''(z_{\gamma_n})}{4\pi\zeta'(z_{\gamma_n})} + F'_{\gamma_n}(z_{\gamma_n}), \tag{11}$$

where

$$F'_{\gamma_n}(z_{\gamma_n}) = \zeta'\left[\frac{\mathrm{d}w}{\mathrm{d}\zeta} + \frac{i\gamma_n}{2\pi}\frac{1}{\zeta - \zeta_{\gamma_n}}\right]. \tag{12}$$

2.4 Kinematics of the incident and free vortices

Similarly, the complex velocity of the incident line vortex at s_Γ is (7)

$$\frac{\mathrm{d}s^*_\Gamma}{\mathrm{d}t} = -\frac{i\Gamma\zeta''(s_\Gamma)}{4\pi\zeta'(s_\Gamma)} + F'(s_\Gamma), \tag{13}$$

where

$$F'_\Gamma(s_\Gamma) = \zeta'\left[\frac{\mathrm{d}w}{\mathrm{d}\zeta} + \frac{i\Gamma}{2\pi}\frac{1}{\zeta - \zeta_\Gamma}\right]. \tag{14}$$

Also, the equation of motion for each of the $n-1$ free vortices is

$$\frac{\mathrm{d}s^*_{\gamma_k}}{\mathrm{d}t} = -\frac{i\gamma_k\zeta''(s_{\gamma_k})}{4\pi\zeta'(s_{\gamma_k})} + F'_{\gamma_k}(s_{\gamma_k}), \tag{15}$$

where

$$F'_{\gamma_k}(s_{\gamma_k}) = \zeta'\left[\frac{\mathrm{d}w}{\mathrm{d}\zeta} + \frac{i\gamma_k}{2\pi}\frac{1}{\zeta - \zeta_{\gamma_k}}\right]. \tag{16}$$

2.5 Airfoil motion and loads

The airfoil moves aeroelastically under its lift force and the equation of motion of the elastic mount,

$$m\frac{d^2h}{dt^2}+c_d\frac{dh}{dt}+k_hh=-L', \tag{17}$$

where $h(t)$ denotes the vertical displacement of the airfoil (postive downward). The airfoil suspension is modeled as a linear harmonic oscillator with mass m, damping coefficient c_d, and spring stiffness k_h. The unsteady lift force L' is determined by (10):

$$L'=\rho U\Gamma_a(t)+\rho\int_0^c\frac{\partial}{\partial t}\Gamma_a(x,t)\,\mathrm{d}x. \tag{18}$$

The system of dynamical equations is formed from Eqs. (9), (10), (13) and (15), which consists of $2(n+2)$ first-order ordinary differential equations for the position $(s_{x_\Gamma}(t),s_{y_\Gamma}(t))$ of the incident line vortex, the positions $(s_{x_{\gamma_n}}(t),s_{y_{\gamma_n}}(t))$ of n trailing-edge vortices, and the instantaneous airfoil displacement $h(t)$ and the velocity $V(t)$. The system of equations is marched forward in time using a fourth-order Runge-Kutta algorithm. Once solved, the results are mapped into the physical z-plane by using $z(t)=s(t)+ih(t)$.

2.6 Acoustic emission

The aerodynamic sound problem at low Mach numbers can be solved by the Powell-Howe acoustic analogy (7, 11)

$$\left(\frac{1}{c_0^2}\frac{\partial^2}{\partial t^2}-\nabla^2\right)B=\mathrm{div}(\boldsymbol{\omega}\wedge\mathbf{v})+\frac{\mathrm{d}V}{\mathrm{d}t}\delta(y), \tag{19}$$

where B is the stagnation enthalpy per unit mass of the fluid (12) and c_0 is the isentropic speed of sound. The first term on the right hand side denotes the vorticity contribution via the divergence of the Lamb vector, and the second term is the airfoil motion contribution. In the acoustic far field, the acoustic pressure and stagnation enthalpy are related by the linearized approximation

$$p(\mathbf{x},t)\approx\rho B(\mathbf{x},t). \tag{20}$$

The acoustic pressure can be written as

$$p(\mathbf{x},t)=p_v(\mathbf{x},t)+p_\omega(\mathbf{x},t), \tag{21}$$

where $p_v(\mathbf{x},t)$ is the acoustic pressure due to the airfoil motion,

$$p_v(\mathbf{x},t)\approx\frac{2\rho\lambda^2\cos\theta}{\sqrt{2c_0|\mathbf{x}|}}\frac{\partial^2}{\partial t^2}\int_{-\infty}^{[t]}\frac{\mathrm{d}h/\mathrm{d}t}{\sqrt{[t]-\tau}}\,\mathrm{d}\tau, \tag{22}$$

and $p_\omega(\mathbf{x},t)$ denotes the contribution from all vortices including the incident vortex and shedding vortices, which can be calculated using Howe's formula (7),

$$p_\omega(\mathbf{x},t)\approx\frac{-\rho\omega x_j}{2\pi\sqrt{2c_0}|\mathbf{x}|^{(3/2)}}\frac{\partial}{\partial t}\int_{-\infty}^{[t]}\left(\frac{\mathrm{d}x}{\mathrm{d}\tau}\frac{\partial Y_j}{\partial y}-\frac{\mathrm{d}y}{\mathrm{d}\tau}\frac{\partial Y_j}{\partial x}\right)_{z(\tau)}\frac{\mathrm{d}\tau}{\sqrt{[t]-\tau}}. \tag{23}$$

Here ω is the vortex strength, $x_j/|\mathbf{x}|$ denotes the observer direction θ, where $\sin\theta=x_1/|\mathbf{x}|$ and $\cos\theta=x_2/|\mathbf{x}|$, $\mathbf{x}$ is the observer location in the far field ($|\mathbf{x}|\to\infty$), $[t]=t-|\mathbf{x}|/c_0$ is the acoustic retarded time, t denotes the observer time, and τ is the source time. Y_j $(j=1,2)$ are the components of the Kirchhoff vector that are established from the conformal mapping,

$$Y_1=\mathrm{Re}\,(\zeta+1/\zeta)\quad\text{and}\quad Y_2=\mathrm{Re}\,\{-i(\zeta-1/\zeta)\}. \tag{24}$$

The integrals in Eq. (23) can be evaluated numerically once the path of the vortex $z(\tau)=x(\tau)+iy(\tau)$ has been determined.

3 RESULTS

In this section we first compare the results of a simpler case against Manela's work (3) to validate the mathematical framework, then plot new findings for the aeroelastic case. The model equations are nondimensionalized by $\bar{x} = x/(2\lambda)$, $\bar{y} = y/(2\lambda)$, $\bar{t} = Ut/(2\lambda)$, and $\Pi([\bar{t}]) = p(\mathbf{x},t)\sqrt{8|\bar{\mathbf{x}}|}/(\rho U^2\sqrt{M})$, which produce the following parametric groups that define the numerical simulations (13):

$$\overline{\Gamma} = \frac{\Gamma}{4\pi U\lambda},\ \overline{\omega}_n = \frac{2\lambda\omega_n}{U},\ \mu = \frac{4\rho_a l_t}{\pi\rho c},\ \xi = \frac{c_d}{2m\omega_n}.$$

The last three parameters are related to the airfoil suspension, where ρ_a is the airfoil density, $\omega_n = \sqrt{k_h/m}$ is the natural frequency of the suspension. The airfoil chord length and λ are related by $c = 3\lambda - 2f_{x0} - \lambda^2/(2f_{x0} - \lambda)$, and $M = U/c_0$ is the Mach number.

3.1 Verification of simulations

Consider the degenerate case of the generalized model in Fig. 1 of a fixed, flat airfoil of length 4λ immersed in a uniform flow with speed U in the x-direction. An incident line vortex of constant strength $\overline{\Gamma} = 0.2$ is released into the flow at the initial instant in time ($\bar{t} = 0$) at position $(\bar{x}_0, \bar{y}_0) = (-20, 0.2)$ and advects freely over the airfoil. This scenario has been previously investigated by Manela (4) and furnishes a verification case for the more general framework developed in this paper. Figure 3(a) illustrates the comparison of the numerical results for the nondimensional acoustic pressure measured directly above a stationary flat plate or a stationary Joukowski airfoil at $\theta = \pi/2$, where the solid curve agrees with Fig. 3(c) of Manela (4).

3.2 Aeroelastic case

Now consider the case of an incident vortex past by a Joukowski airfoil under aeroelastic motion, as illustrated in Figure 1. The Joukowski airfoil has 12% thickness and zero angle of attack. The initial strength and location of the incident vortex are the same as in Section 3.1, and the additional dimensionless parameters for the aeroelastic case are the damping ratio $\xi = 0$, reduced natural frequency $\overline{\omega}_n = 0.5$, and mass ratio $\mu = 10$. The sound produced by the unsteady suction ($\theta = \pi/2$) in different aspects is shown in Figure 3(b) and (c), respectively. In Figure 3(b), the solid curve denotes the incident vortex acoustic contribution, and the dashed curve denotes the wake contribution which includes the effect of 12 Brown-Michael vortices that are shed by the trailing edge over the course of the simulation. The reduced pressure of the incident vortex contribution decreases when the incident vortex passes by the leading edge, and the pressure of the wake contribution starts to fluctuate due to more vortices shedding from the airfoil trailing edge. After the incident vortex passes by the trailing edge, the wake contribution and the incident vortex contribution start to balance together with same strength in opposite signs and yield a net zero total acoustic pressure in long times, as illustrated in Figure 3(c). Compared with the total sound for a stationary flat and thick Joukowski airfoils in Figure 3(a), the result in Figure 3(c) shows that aeroelastic effects have a modest slight influence in the total sound for the parameters considered here. However, the comparison of flat airfoil and Joukowski airfoil in Figure 3(a) shows that the airfoil thickness controls significantly the peak noise due to the acceleration of the vortex in the leading-edge interaction. Figure 3(d) presents the sound observed along a different observation angle ($\theta = 0$) produced by the unsteady lift contributions of the incident vortex, the wake, and the airfoil motion.

4 CONCLUSIONS

An analytical model for the aeroelastic interaction of an incident vortex and a symmetric Joukowski airfoil is formulated in this paper. The aeroelastic vortex dynamics study by (6) is extended to study the corresponding acoustic emissions using the Powell-Howe acoustic analogy. The acoustic signature for the special case of a stationary flat-plate airfoil is verified against available results in the literature. New acoustic results show that the airfoil thickness controls significantly the total sound, while a modest difference in total sound is observed

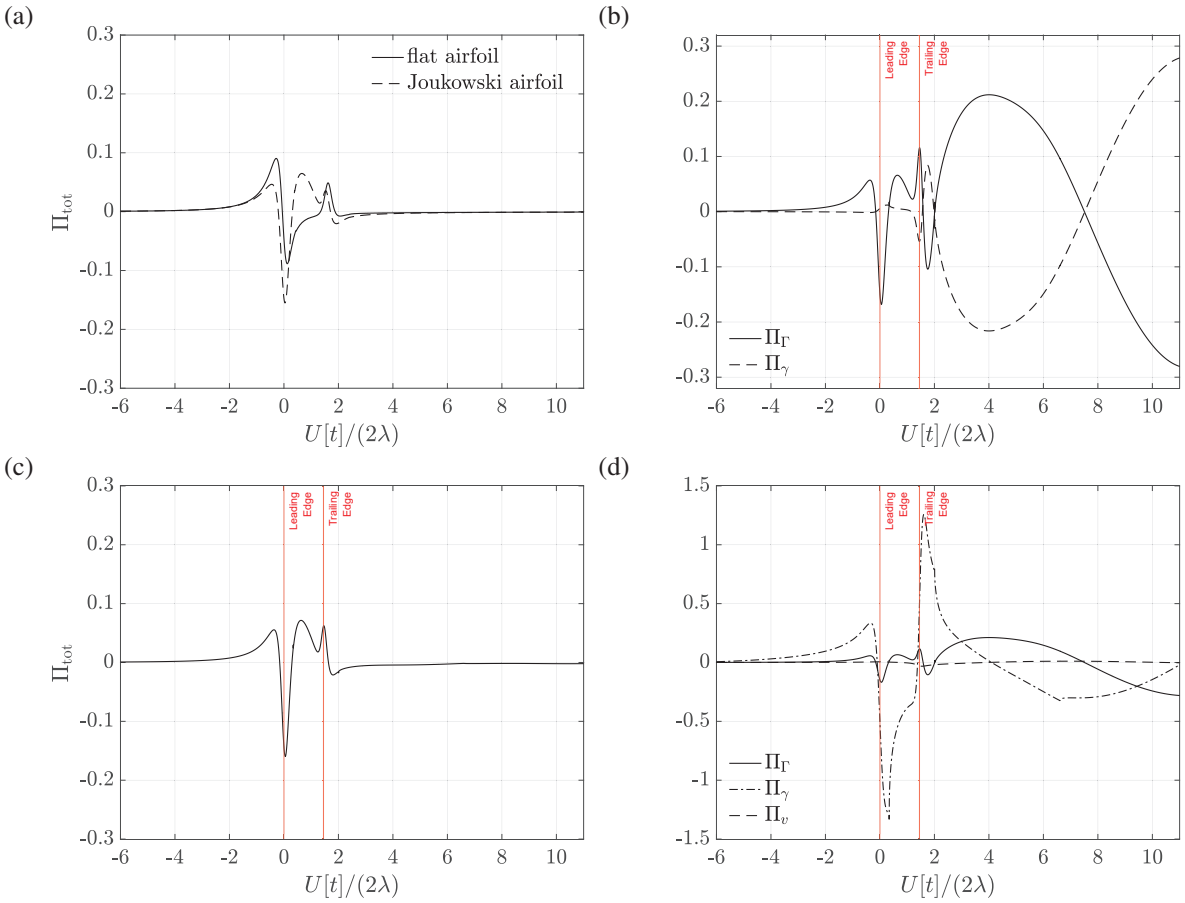

Figure 3. Acoustic radiation of a line vortex encountering a stationary flat-plate airfoil or a Joukowski airfoil with 12% thickness: (a) comparison of total acoustic radiation for the stationary flat and Joukowski airfoils along $\theta = \pi/2$; (b) acoustic contributions of incident vortex (Π_Γ) and wake ($\Pi_\gamma = \sum_{k=1}^{k=12} \Pi_{\gamma_k}$) for a Joukowski airfoil under aeroelastic motion along $\theta = \pi/2$; (c) total normalized acoustic pressure for a Joukowski airfoil under aeroelastic motions observed at angle $\theta = \pi/2$; (d) acoustic contributions of the incident vortex (Π_Γ), vortical wake (Π_γ), and the airfoil motion (Π_v) for a Joukowski airfoil under aeroelastic motion, as observed along $\theta = 0$. For the aeroelastic simulations in (b-d), $\xi = 0$, $\overline{\omega}_n = 0.5$, and $\mu = 10$.

in the comparison of stationary and aeroelastic cases for the parameters considered. A complete parameter sweep of the aeroelastic cases is the subject of ongoing research to determine conditions for minimum noise production and the associated dynamics of the gust-airfoil interaction.

ACKNOWLEDGEMENTS

This work was supported in part by the Air Force Office of Scientific Research under AFOSR grant FA9550-15-1-0148, monitored by Drs. Douglas Smith and Gregg Abate, and by the National Science Foundation under awards 1805692 and 1846852, monitored by Dr. Ronald Joslin.

References

[1] Brown CE, Michael WH. Effect of leading-edge separation on the lift of a delta wing. Journal of the Aeronautical Sciences. 1954;21(10):690–694.

[2] Howe MS. Emendation of the Brown & Michael equation, with application to sound generation by vortex motion near a half-plane. Journal of Fluid Mechanics. 1996;329:89–101.

[3] Manela A, Huang L. Point vortex model for prediction of sound generated by a wing with flap interacting with a passing vortex. Journal of the Acoustical Society of America. 2013;133(4):1934–1944.

[4] Manela A. Nonlinear effects of flow unsteadiness on the acoustic radiation of a heaving airfoil. Journal of Sound and Vibration. 2013;332(26):7076–7088.

[5] Riso C, Riccardi G, Mastroddi F. Nonlinear aeroelastic modeling via conformal mapping and vortex method for a flat-plate airfoil in arbitrary motion. Journal of Fluids and Structures. 2016;62:230–251.

[6] Chen H, Jaworski JW. Vortex interactions with Joukowski airfoil on elastic supports. In: AIAA Fluid Dynamics Conference, Atlanta, GA. Paper AIAA-2018-2907; 2018. .

[7] Howe MS. Theory of vortex sound. Cambridge University Press, United Kingdom; 2003.

[8] Batchelor GK. An introduction to fluid dynamics. Cambridge University Press, United Kingdom; 1967.

[9] Howe MS. Acoustics and aerodynamic sound. Cambridge University Press, United Kingdom; 2014.

[10] Katz J, Plotkin A. Low-speed aerodynamics. 2nd ed. Cambridge University Press, United Kingdom; 2001.

[11] Howe MS. Acoustics of fluid-structure interactions. Cambridge University Press; 1998.

[12] Howe MS. Contributions to the theory of aerodynamic sound, with application to excess jet noise and the theory of the flute. Journal of Fluid Mechanics. 1975;71(4):625–673.

[13] Chen H, Jaworski J. Aeroelastic trajectory selection of vortex gusts impinging upon Joukowski airfoils. In: AIAA Scitech 2019 Forum; 2019. p. 0897.